# Ripples at Edges of Blooming Lilies and Torn Plastic Sheets

Thomas Portet,[1] Zachary R. Cohen,[1*] Gunnar J. Goetz,[1*] Nicole Panek,[1] Peter N. Holmes,[1] Sean A. Stephens,[2] Tamas Varga,[2] and Sarah L. Keller[1**]

[1]Department of Chemistry, University of Washington – Seattle, Seattle, WA, 98195, USA

[2]Pacific Northwest National Laboratory – EMSL, Richland, WA, 99352, USA

[*]Authors contributed equally

[**]To whom correspondence should be addressed; E-mail: slkeller@uw.edu

**Running title:** Ripples at the edges of lily petals

**Keywords:** morphogenesis, petal shape, rippling, buckling, tomography

**Abstract:** Ripples arise at edges of petals of blooming *Lilium casablanca* flowers and at edges of torn plastic sheets. In both systems, ripples are a consequence of excess length along the edge of a sheet. Through the use of time-lapse videos of blooming lilies and published images of torn plastic sheets, we find that ripples in both systems are well-described by the scaling relationship $a \propto \sqrt{w(L-w)}$, where $a$ is amplitude, $w$ is wavelength, and $L$ is arc length. A phenomenological relationship previously reported for self-similar ripple patterns, namely $\langle a \rangle \propto \langle w \rangle$, can be recovered by assuming that buckling stress is constant. Excess length along petal edges can also influence their overall Gaussian curvature, such that petals invert from a cup shape to a saddle shape upon blooming. Previous simulations of these shape changes have assumed that petal thickness decreases at least quadratically. Here, we evaluate tomograms of several varieties of lily buds and find that this assumption is valid along the short axis of the buds, but not the long axis. A challenge of employing traditional tomography methods to measure petal thickness is that the sample is destroyed; a single bud cannot be followed through the entire blooming process. To address this challenge, we provide proof of principle that the non-destructive, label-free method of X-ray tomography produces high-contrast 3-dimensional scans on time scales short enough to follow lily blooming.

**Significance Statement:** By adopting appealing shapes, flowers enlist humans to disseminate their progeny. As lilies bloom and change shape, their genes determine how much faster edges of petals grow than centers. One physical consequence of edge growth is inversion of petals from cup shapes to saddles. This transformation is difficult to image by standard techniques. We show that X-ray tomography successfully images lilies in a label-free and relatively nondestructive manner. A second consequence of edge growth is that ripples appear at petal edges. We find that ripple amplitudes, wavelengths, and arc lengths are related by an equation for buckling of sheets under nonuniform stresses. The same equation should apply to all ripples driven by edge growth, whether in biological or artificial materials.

## INTRODUCTION

Morphological changes in flowers elegantly connect the abstract beauty of mathematics and the tangible beauty of nature. Two recent studies inspired our current investigation of lilies. In the first, the authors applied a growth hormone to the edge of flat plant leaves to create ripples (*1*). In the second, the authors combined surgical manipulations of *L. casablanca* lilies, numerical simulations, and exact calculations to argue that lily blooming is driven primarily by edge growth (*2*). In this mechanism, growth along edges of lily tepals (colloquially termed petals) is enhanced with respect to tepal faces, such that excess length accumulates along edges. Blooming of lilies from closed buds to six-pointed stars (Fig. 1) entails curvature reversal of tepals from cup shapes to saddle shapes and may be accompanied by the emergence of ripples at the edges of the tepals.

Flowers that exhibit ripples along their edges, whether lily tepals or daffodil trumpets, do not necessarily genetically encode rippling beyond driving a generalized edge growth that results in blooming (*1, 3*). Ripples are observed in a wide class of systems that accommodate excess length along an edge. Simulations of elastic ribbons with high rates of edge growth result in rippled morphologies (*4*). Similarly, polymer disks that undergo nonuniform swelling can buckle at their rippled edges, as can annular thin strips undergoing nonuniform stresses (*5–9*). In more quotidian examples, knitters create ripples by inserting stitches at edges, and ripples form at the new edges of a torn plastic sheet (*1, 3, 10–12*).

Here, our central goal is to quantitatively explain the shape of ripples in sheets undergoing edge growth. When rippling is the result of buckling, a simple scaling law arises that relates a ripple's amplitude $a$, wavelength $w$, and arc length $L$. The exact form of the scaling relationship depends on whether stress is constant. We test which form of scaling applies to single ripples at edges of lily tepals (which we might expect to have nonuniform stresses) and torn plastic sheets (which we might expect to be uniform at long length scales, but perhaps not at short ones). Overall, our data support a view that biology and physics work in tandem to create lily tepals with delicate ripples along their edges: genes regulate the rate of edge growth, and buckling within each tepal converts this growth into wavy edges (*13*).

Our second goal is to image lily buds, for two reasons. To enable future calculations of cur-

vature reversal in tepals from realistic starting configurations, we use surgical tomography to record 3-dimensional shapes of closed buds of several lily varieties. To enable future imaging of the full 3-dimensional shape changes of a single lily, we establish that label-free X-ray tomography collects high-contrast scans on time scales an order of magnitude shorter than blooming. Each of these methods presents an advantage: surgical tomography is broadly accessible, and X-ray computed tomography is less destructive.

One could ask whether ripples confer an evolutionary advantage to lilies. Michael Pollan argues in *The Botany of Desire* that genetic expression in many plants is influenced by the aesthetic and culinary tastes of humans. Evolution in plants records both natural history and human history. Pollan writes how a tulip with "petals attenuated like sabers, contains detailed instructions on how to best catch the eye not of a bee but of an Ottoman Turk; it has something to tell us about that age's idea of beauty" (*14*). Judging from how common it is to find rippled lilies in Seattle's gardens, which lie far from the flowers' ancestral homes in Asia, it appears that lilies have successfully harnessed edge growth and buckling in an evolutionary strategy that has motivated humans to feed them, propagate them, and extend their range.

## METHODS

### Videos and measurement uncertainty

Videos were collected of lilies blooming and rippling. *L. casablanca* and *L. stargazer* varieties, which are Division VII oriental hybrids, were trimmed so only one outer tepal remained, as in Fig. S1. The remaining tepal was imaged from the side at constant illumination of 60 $\mu\mathrm{mol}/\mathrm{m}^2\mathrm{s}$ and $20^\circ\mathrm{C}$ in a time-lapse chamber previously described by Stewart Lilley *et al.* (*17*). Image capture started a few hours after blooming commenced (before rippling) and stopped when ripples became static. Measurement uncertainties for $a$, $w$, and $L$ are equivalent and on the order of $\pm 0.05$ cm. Uncertainties arise mainly because tepal edges deviate from the camera's focal plane due to flower motion or shape changes. Smaller uncertainties arise from image analysis, which combines manual detection of ripple zeniths and nadirs with automated edge detection by ImageJ (https://imagej.nih.gov/ij).

### Tomography of closed lily buds

Closed buds of lilies (oriental hybrids and tiger lilies, *L. lancifolium*) were loosely wrapped in Teflon tape and held with the tip downward on a cylindrical pedestal. A circular rim on the

pedestal protruded $1.8 \pm 0.2$ mm (for *L. speciosum* (*var. alba*)) or $\sim 3$ mm (for other lilies) above the center. Buds were sectioned by clamping a tomography blade in a vice-grip, and using the pedestal rim as a guide along which the blade slid to cut the bud. After each slice was cut, the cross section of the remaining bud was imaged using a standard digital camera (PowerShot SD1100 IS; Canon, Melville, NY) or, for *L. speciosum* (*var. alba*) a cell phone (iPhone 7, Apple, Cupertino, CA).

**Image analysis of tomograms**

In each photograph of lily slices, areas of outer tepals and an H-shaped scale bar were traced by hand in Photoshop (Adobe, San Jose, CA) to produce binarized images. The scale bar was converted from pixels to mm using functions from the scikit-image library (*18*). Specifically, "skeletonize", "label", and "regionprops_table" were used to identify, isolate, and measure the length of the scale bar. The three outer tepals were then identified within the binarized image, and each tepal image was cropped and placed into its own file using the scikit-image function library. Images of all slices of each tepal were then grouped in ordered sets corresponding to the original position of the slice within the bud. Each binarized tepal image was then skeletonized, and tepal thicknesses were measured along a line perpendicular to the skeleton (Fig. S2). The length of the semiminor axis, $b$, of each tepal was defined to be the maximum distance between points on the skeleton, and defined to be at $x = 0$. The length of the semimajor axis, $c$, was defined to be the distance between $x = 0$ and the tip of the tepal. The authors have made all original Python code available by public license at https://github.com/nicolepanek/2021_LilyProject.

**X-ray microtomography**

X-ray computed tomography was conducted at the Environmental Molecular Sciences Laboratory at the Pacific Northwest National Laboratory in Richland, WA. Each lily was mounted and kept hydrated in a rotating chuck that held a tube filled with water. The X-ray power settings were $85\ kV$ and $250\ \mu A$. Lilies were translated vertically to image sequential slices, in $0.886\ mm$ steps for a lily bud and $1.1\ mm$ steps for a lily bloom. Individual radiographs were collected with $708\ ms$ exposure times, and 4 frames were recorded per projection, for a total of 3142 projections. Lilies were rotated during the scans to capture 3-dimensional data. The image voxel size for the lily bud was $0.0439\ mm$ and $0.0536\ mm$ for the lily bloom. Each scan was completed in approximately 4 hours. Although exposure to X-rays eventually damages plant tissue, the technique is considered nondestructive.

**Alternative derivation of Eq. 2**

We consider the simple case of a first generation ripple that has no second generation ripples superimposed on it. We model the ripple's edge as a planar curve for which each point has coordinates $(x, f(x))$, where $x \in [-w/2, w/2]$ because the ripple's wavelength is $w$. We assume the ripple is symmetric and pinned at the edges, which means that the function $f$ is smooth, is even, and satisfies boundary conditions of $f(w/2) = f(-w/2) = 0$ and $f(0) = a$. The arc length $L$ of the curve is, by definition, $L = \int_{-w/2}^{w/2} \sqrt{1 + f'(x)^2}\, \mathrm{d}x$, which is simplified via a Taylor expansion to $L \approx w + (1/2) \int_{-w/2}^{w/2} f'(x)^2\, \mathrm{d}x$ for a smooth function $f$. Because the function $f$ is even, its expansion does not contain odd powers and is, to second order, $f(x) \approx a + f''(0)x^2/2$. Using a difference quotient approximation, the second derivative at the origin is $f''(0) \approx -\epsilon(a/w^2)$, with dimensionless factor $\epsilon$. Direct integration of $f'^2$ yields $a \propto \sqrt{w(L-w)}$, which is Eq. 2. If arc length were directly proportional to wavelength, as in a small-angle approximation for ripples of small amplitude, then insertion of $L \propto w$ (where $L > w$) in Eq. 2 would yield $a \propto w$. In practice, $L$ is difficult to measure in a rippled edge that has additional generations of ripples superimposed on it.

## RESULTS AND DISCUSSION

### Rippling

Ripples in lily tepals appear singly or in multiple generations. Fig. 1C shows a large, first-generation ripple decorated with smaller, second-generation ripples. These patterns are reminiscent of self-similar ripples at edges of torn plastic sheets. Sharon *et al.* (*11*) have related the amplitudes, $a$, and wavelengths, $w$, for five generations of superimposed ripples in plastic sheets, spanning two orders of magnitude, by

$$a \propto w. \tag{1}$$

However, when we attempted to apply Eq. 1 to ripples in lily tepals, we found a poor fit. The fit improved only after averaging all amplitudes and wavelengths within each generation (Fig. 1C-D). Even after averaging, the uncertainty was large; the slope of $log\langle w\rangle$ *vs.* $log\langle a\rangle$ is 1.19 with a 90% confidence interval of $\pm$ 0.63.

The reason that averaging over many ripples leads to a better fit of $a \propto w$ lies in the

equations that describe buckling in thin sheets. The amplitude of a buckled beam scales as $a \propto w\sqrt{strain}$. This equation has previously been applied to sheets under tensile strain (*19*) and attached to compliant supports (*26*). The definition of $strain = (L - w)/w$ yields

$$a \propto \sqrt{w(L - w)}\,. \tag{2}$$

Another way to derive Eq. 2 is to introduce a function $f(x)$ that describes the height at every point on a ripple (see the Methods). The ripple begins at $x = -w/2$ (with zero height), rises to an amplitude $a$ at $x = 0$, and returns to a height of zero at $x = w/2$. The only assumptions that need to be imposed are that the function is smooth and symmetric. By taking a second order Taylor expansion of the function, we find that $a \propto \sqrt{w(L - w)}$.

When strain is constant, Eq. 2 simplifies to $a \propto w$. However, strain is not constant in lilies. Strain due to growth at the edges of *L. casablanca* tepals increases linearly in the direction of the long axis, more than doubling from ∼0.2 at the tepal base to ∼0.5 near the tip, with large standard deviations, on the order of ± 0.1 (*2*). Therefore, for individual ripples in lily tepals, we expect $a \propto \sqrt{w(L - w)}$ to provide a better fit than $a \propto w$.

To test Eq. 2, we collected videos of lilies blooming and rippling. We used *L. casablanca* specimens because buds are large ($\sim 10$ cm), are widely available, and bloom over the course of approximately one day (*16*). We focused on single ripples, which we define as having no higher-order generation ripples superimposed upon them. Single ripples minimize ambiguity in how to define $a$ and $w$. Fig. 2 shows frames of single, 1st-generation ripples at edges of tepals. A movie corresponding to Fig. 1B appears in the Supporting materials (Movie S1). Ripples appear at higher densities near the tips of tepals than at their stems (Fig. 2), consistent with greater edge growth near the tip.

As lilies bloomed, we tracked each ripple's amplitude, wavelength, and arc length over time (Movie S1 in the Supporting materials). Ripple amplitudes and arc lengths increase over time (Fig. 3A and S4). In contrast, wavelengths are approximately constant over time (Fig. 3B), making boundary conditions of $a = 0$ at $x = \pm w/2$ straightforward to implement. We find that ripple amplitude, wavelength, and arc length are related by Eq. 2 for single ripples in tepals of

*L. casablanca* (Fig. 3C). All other scaling relationships fail in which amplitude $a$ is proportional to a simple expression with units of length, namely $w$, $L$, $\sqrt{Lw}$, $L + w$, or $L - w$ (Fig. 4). For clarity, Fig. 3 displays data for only single ripples, excludes ripples with amplitudes $\leq 0.1$ cm, and does not show experimental uncertainties. Full data sets with experimental uncertainties appear in Fig. S3.

For any sheet with edge growth, whether a lily tepal or a plastic film, determining whether the relationship $a \propto w$ fits ripple shapes as well as the relationship $a \propto \sqrt{w(L-w)}$ does is a means of assessing the length scale of inhomogeneities. The plastic sheet of Sharon *et al.* (*11*) was presumably uniform before it was torn. As it ripped, inhomogeneities may have arisen, which would be most evident in ripples of the same length scale. To test for these inhomogeneities, we analyzed raw images of $5^{th}$ generation single ripples from Sharon *et al.* (*11*), as in Fig. S5 and S6. These small ripples have wavelengths on the order of $100$ $\mu$m and are not fit by $a \propto w$. (Fig. 5A, slope of -0.12 $\pm$0.27). We expected that larger ripples would be insensitive to inhomogneities, and found a better, but still only approximate agreement with $a \propto w$, even at length scales larger than $1$ $mm$ (Fig. 6A, slope = 1.1 $\pm$0.037). In other words, strain was not constant while the sheet was torn, either at the sub-millimeter length scales of 5th generation ripples (where local inhomogeneities might be expected) or in larger ripples approaching $\sim 10$ mm (where strains might be expected to average out). Sharon *et al.* (*11*) reported a closer fit, which likely arose because their data were binned and averaged. In contrast, the relationship $a \propto \sqrt{w(L-w)}$ from Eq. 2 holds for all five generations of ripples in torn plastic sheets (Fig. 6B, slope = 1.0 $\pm$0.0083), including the smallest ripples (Fig. 5B, slope = 0.63 $\pm$0.095). The excellent fit to Eq. 2 indicates that the second order Taylor expansion used in the derivation Eq. 2 is sufficient.

A separate question is how the shape descriptors of ripples evolve over time. In rippled 2-dimensional sheets, preferential wavelengths emerge from a competition between stretching and bending – the former favors short wavelengths, and the latter favors longer ones (*19*). As a tepal edge grows, small, first-generation ripples appear at sites separated by a distance $w$ that presumably arises from minimization of the stretching and bending energies. Our data in Fig. S4 show that $w$ remains approximately constant, implying that the tepal's elastic modulus does not change significantly over time. As a tepal edge grows, the arc length $L$ of ripples increases. The tepal reacts to the excess edge length by buckling, so ripple amplitude $a$ also grows with time,

where $a$ scales as $\sqrt{w(L-w)}$.

Rippling is largely independent of the original (pre-rippled) length of the tepal, which is consistent with the notion that ripples arise from local strains. In Movies S2-S4 in the Supporting materials, ripples appear roughly synchronously in outer tepals that are $67\%$, $75\%$, and $100\%$ of their original length. In some blooms (Movies S2 and S3), ripples arise when all tepals are in cup shapes, whereas in others (Movie S4), rippling begins only after larger shape changes. Rare exceptions occur; Fig S8 shows a bloom in which ripples in the shortest tepal have smaller amplitudes than ripples in longer tepals. Similar differences in amplitudes occasionally occur when all tepals are the same length.

**Blooming**

Whereas *L. casablanca* lilies are characterized by ripples at tepal edges, *L. lancifolium*, tiger lilies, are not (Fig. 7). In both varieties, blooming entails a reversal of curvature as the tepals progress from cup to saddle shapes. In a model by Liang and Mahadevan (*2*), edge growth drives this curvature reversal. The model assumes that the tepal is initially an elliptical cup with a lenticular cross-section of thickness, $t$, that decreases at least quadratically along both the long and short axes of the tepal such that $t = t_0(1 - x^n/c^n - y^n/b^n)$, where $t_0$ is the maximum thickness, $c$ is the semi-major axis of the elliptical cup, $b$ is the semi-minor axis, and $n \geq 2$. The assumption that tepal thickness varies at least quadratically renders tepal edges free of forces and torques (*2*).

Here, we tested the model's assumption by collecting tomograms of buds from several lily varieties and measuring tepal thickness (Fig. 7 and Movies S5-8 in the Supporting materials). The lily tepals vary in their overall size, their aspect ratio, and their final curvatures after blooming. For some varieties, each tepal in a bud is well approximated by an elliptical cup. However, for others, tepal edges double back toward the center such that thickness is double-valued in $y$ and nonzero at $y = \pm b$. If we truncate tepals before they double back, we find that tepal thickness generally decays at least as faster as $t = t_0(1 - y^2/b^2)$ in the semi-minor direction (Fig. 7). However, thickness is roughly constant or only slowly decreases in the semi-major direction. Both of these results are related to the thick, woody spine at $y = 0$. The center of the spine has a roughly uniform thickness along the semi-major direction. Away from the spine, tepal

thickness decreases roughly linearly with $y$ for all lily varieties. Although the spine's uniform thickness means that the model's assumptions do not entirely represent the biological system, the result does not have any bearing on whether or not edge growth is the primary driver of curvature reversal in tepals. To enhance the realism of future simulations, we have compiled a set of tomogram slices for a *L. lancifolium* bud in Fig. S7, and we have assembled all slices of the projections in Fig. 7 in movies in the Supporting materials.

Tepal shapes in Fig. 7 were found by hand-sectioning lily buds. This process is straightforward and could be easily adapted for citizen science projects. However, it is time-consuming and destroys the sample so that a single bud cannot be followed through the blooming process. Moreover, after a lily has begun to bloom, it is too fragile to hand-section; the flower would have to be immobilized in resin and sectioned in a microtome. A related approach for quantifying the shape and edge growth of a tepal after a lily has begun to bloom is to cut thin strips from the edge of a ripple. When disconnected from the larger sheet, strips of this type curl into a flat annulus. Given physical values that characterize individual strips, numerical minimizations of the strip's energy result in rippled solutions (*7, 8*). However, cutting strips also destroys the sample.

To overcome these challenges, we tested the feasibility of an alternative, non-destructive technique. Fig. 8 shows a label-free X-ray computed tomogram of a lily bud and reconstructed bloom. These images (as well as Fig. S9 and Movie S9 in the Supporting materials) demonstrate strong contrast in X-ray absorption between the lily tissue and the surrounding air. In some images, individual cells are resolvable, which could be used to discover if the biological mechanism of edge growth involves changes in cell size, cell shape and/or cell number. Higher contrast and shorter acquisition times might be achievable if a contrast agent (e.g., iodine) were added to the aqueous solution that hydrates the lily stems. Here, acquisition times were on the order of hours. Computed X-ray tomography has previously been used to image delicate biological structures of air-water interfaces in lungs (*23*).

## CONCLUSIONS

Our results fit within a framework that edge growth can lead to ripples and the resulting

"length scales could be set by elasticity and geometry rather than by explicit genetic encoding" (*3*). No constraints are set on the method by which a lily tepal achieves edge growth; any biological mechanism is allowed. Here, we find that the amplitude, wavelength, and arc length of ripples are excellently fit by the equation of a buckling beam, $a \propto \sqrt{w(L-w)}$. An alternative equation of $a \propto w$, does a poor job of fitting ripples in lilies (which could be expected) and across all length scales of torn plastic sheets (which was not expected). Because ripples occur at the edges of many types of leaves and petals (*1*), assessment of whether ripples are well described by $a \propto w$ is a widely applicable method of determining if nonuniform stresses act in these biological materials.

Edge growth is not the only possible mechanism of blooming. Historically, lily blooming has also been attributed to enhanced expansion of cells on the adaxial (interior) face of tepals with respect to cells on the abaxial (exterior) face. Bieleski *et al.* assert that any differential expansion of this type must play a minor role because it follows (rather than precedes) the onset of blooming (*15*). Changes in the angle and curvature of the midrib—the tepal's woody spine—also contribute to blooming (*2, 15*). In this manuscript, we have shown that X-ray tomography can be used in a nondestructive and label-free manner to image lilies on time scales of hours, which is commensurate with time scales for budding. In the future, X-ray tomography could be used to assess relative sizes, shapes, and growth rates of cells throughout the tepal.

This manuscript has focused on edge growth in lilies, which is only one example of how biology and physics complement each other to influence plant shape. Some flower types are subject to directional growth, as in *Antirrhinum* (snapdragon) (*20*), and cell-shape anisotropy, as in *Aquilegia* (columbine) (*21*). Moreover, rippling can be influenced by external forces. The magnitude of water flow around long kelp leaves influences whether growing blades adopt flat or rippled morphologies, and pushing on the blade's edge can alter the wavelength and amplitude of ripples (*25*). Similarly, in lotus leaves, the wavelength of edge ripples and the overall leaf shape are influenced by whether the leaves rest on a water surface or not (*24*). Our results and these prior studies illustrate ways that biological morphologies could be recapitulated in biomimetic systems and tuned by physical factors.

**SUPPORTING MATERIAL**

9 movies, and 9 figures are available.

## AUTHOR CONTRIBUTIONS

T.P. and S.L.K. designed research. T.P., T.V., S.A.S., and S.L.K. collected data. T.P. derived equations. Z.R.C., G.J.G., and N.P. wrote original code. T.P., Z.R.C, G.J.G., N.P., and P.N.H. analyzed data. T.P., Z.R.C., G.J.G., N.P., S.A.S., T.V., and S.L.K. produced images and figures. S.L.K. wrote the paper, based on an early version written in collaboration with T.P.

## DECLARATION OF INTEREST

The authors declare no competing interests.


## ACKNOWLEDGMENTS

We thank Jennifer Nemhauser and her group for access to and assistance with time-lapse imaging. We thank Julie Graber for the loan of a time-lapse camera. Lilies were from local florists or the kind gifts of Dianne Carlson, Marie Davis, Elizabeth Harasek, and Beth Hammermeister. We thank L. Mahadevan for his engaging seminar that inspired this study, and we thank Jonathan Litz and Ido Levin for their critiques of our manuscript. We are grateful for correspondence with Harry Swinney, Michael Marder, Benoit Roman, and especially Eran Sharon for his assessment that we "are probably right" that data in Fig. 1A of (*11*) were averaged, with error bars of standard deviations. We thank every one of our anonymous reviewers for outstandingly constructive feedback, especially for suggesting the alternate derivation below Eq. 2. S.L.K. thanks the Whitely Center at UW's Friday Harbor Laboratories for a writing retreat. This research was funded by NSF MCB-0744852 and MCB-1925731 to the Keller Lab. T.P. was funded by the Raymond and Beverly Sackler Foundation and the Fondation Bettencourt Schueller. X-ray tomography was performed at EMSL, a DOE Office of Science User Facility sponsored by the Biological and Environmental Research program, through rapid access proposal 47680 coordinated with Mark E. Bowden.

# References


1. Sharon, E.., M. Marder, and H. L. Swinney. 2004. Leaves, flowers and garbage bags: Making waves. American Scientist. 92:254-261.

2. Liang, H., and L. Mahadevan. 2011. Growth, geometry, and mechanics of a blooming lily. Proc. Natl. Acad. Sci. USA. 108:5516-5521.

3. Sharon, E., B. Roman, and H. L. Swinney. 2007. Geometrically driven wrinkling observed in free plastic sheets and leaves. Phys. Rev. E. 75:046211.

4. Liang, H., L. Mahadevan. 2009. The shape of a long leaf. Proc. Natl. Acad. Sci. USA. 106:22049-22054.

5. Kim, J., J. A. Hanna, M. Byun, C. D. Santangelo, R.C. Hayward. 2012. Designing Responsive Buckled Surfaces by Halftone Gel Lithography. Science. 335:1201-1205.

6. Davidovitch, B., R.D. Schroll, D. Vella, M. Adda-Bedia, and E.A. Cerda. 2011. Prototypical model for tensional wrinkling in thin sheets. Proc. Natl. Acad. Sci. USA. 108:18227-18232.

7. Audoly, B., A. Boudaoud. 2002. 'Ruban a godets': an elastic model for ripples in plant leaves. C.R. Mecanique. 330:831-836.

8. Marder, M., E. Sharon, S. Smith, B. Roman. 2003. Theory of edges of leaves. Europhys. Lett. 62:498-504.

9. Huang, C., Z. Wang, D. Quinn, S. Suresh, K.J. Hsia. 2018. Differential growth and shape in plant organs. Proc. Natl. Acad. Sci. USA. 115:12359-12364.

10. Daniels, K.E., M.W. Elting. 2020. Knitting ripples. Patterns. 1:1-4.

11. Sharon, E., B. Roman, M. Marder, G. S. Shin, H. L. Swinney, 2002. Buckling cascades in free sheets. Nature. 419:579.

12. Audoly, B., A. Boudaoud. 2003. Self-similar structures near boundaries in strained systems. Phys. Rev. Lett. 91:086105.

13. Nath, U., B.C.W. Crawford, R. Carpenter, E. Coen. 2003. Genetic control of surface curvature. Science. 299:1404-1407.

14. Pollan, M., 2002. The Botany of Desire: A Plant's Eye View of the World. New York. Random House.

15. Bieleski, R., J. Elgar, J. Heyes. 2000. Mechanical aspects of rapid flower opening in Asiatic lily. Ann. Bot. 86:1175-1183.

16. Bieleski, R., J. Elgar, J. Heyes, A. Woolf. 2000. Flower opening in Asiatic lily is a rapid process controlled by dark-light cycling. Ann. Bot. 86:1169-1174.

17. Stewart Lilley, J. L., C. W. Gee, I. Sairanen, K. Ljung, J. L. Nemhauser. 2012. An endogenous carbon-sensing pathway triggers increased auxin flux and hypocotyl elongation. Plant Physiol. 160:2261-2270.

18. van der Walt, S., J. L. Schonberger, J. Nunez-Iglesias, F. Boulogne, J. D. Warner, N. Yager, E. Gouillart, T. Yu, scikit-image contributors. 2014. scikit-image: Image processing in Python. PeerJ 2:e453.

19. Cerda, E., L. Mahadevan. 2003. Geometry and physics of wrinkling. Phys. Rev. Lett. 90:074302.

20. Rolland-Lagan, A.-G., J.A. Bangham, E. Cohen. 2003. Growth dynamics underlying petal shape and asymmetry. Nature. 422:161-163.

21. Puzey, J.R., S.J. Gerbode, S.A. Hodges, E.M. Kramer, L. Mahadevan. 2012. Evolution of spur-length diversity in *Aquilegia* petals is achieved solely through cell-shape anisotropy. Proc. Royal Soc. B. 279:1640-1645.

22. Savin, T., N.A. Kurpios, A.E. Shyer, P. Florescu, H. Liang, L. Mahadevan, C.J. Tabin. 2011. On the growth and form of the gut. Nature. 476:57-62.

23. Ritman, E.L.. 2004. Micro-computed tomography – current status and developments. Annu. Rev. Biomed. Eng. 6:185-208.

24. Xu, F., C. Fu, Y. Yang. 2020. Water affects morphogenesis of growing aquatic plant leaves. Phys. Rev. Lett. 124:038003.

25. Koehl, M.A.R., W.K. Silk, H. Liang, L. Mahadevan. 2008. How kelp produce blade shapes suited to different flow regimes: A new wrinkle. Integr. Comp. Biol. 48:834-851

26. Jiang, H., D.-Y. Khang, J. Song, Y. Sun, Y. Huang, J.A. Rogers. 2007. Finite deformation mechanics in buckled thin films on compliant supports. Proc. Nat. Acad. Sci. USA. 104:15607-15612

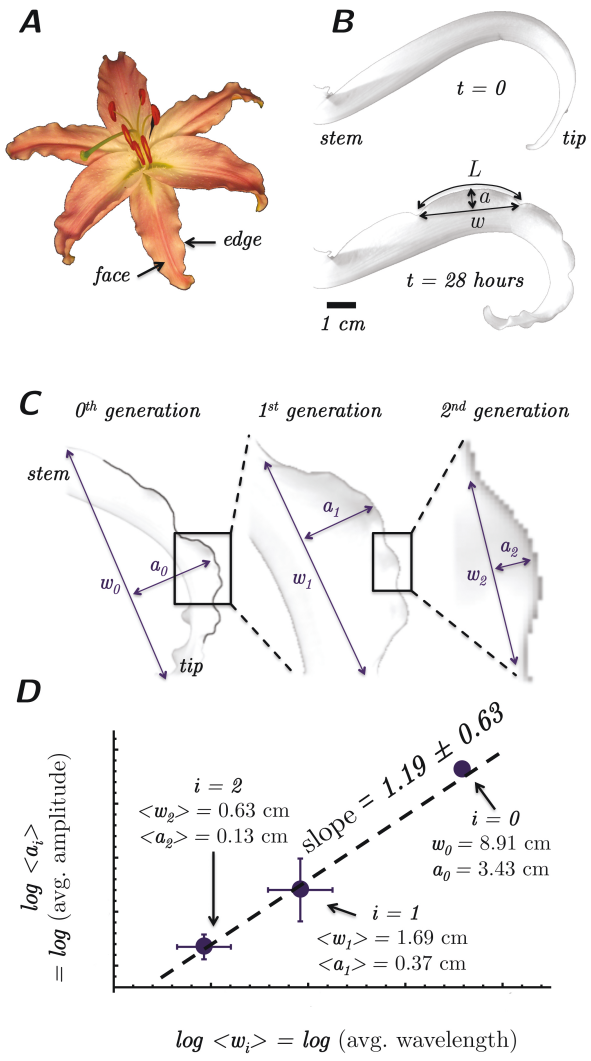


Figure 1: **Self-similar ripples in lilies. A:** Top view of an open stargazer lily with three inner and three outer tepals. **B:** Side view of an outer tepal of *Lilium casablanca* before (top) and after (bottom) edge rippling, with amplitude $a$, wavelength $w$, and arc length $L$. **C:** Examples of an amplitude $a_i$ and wavelength $w_i$ for ripples for each generation $i$. The leftmost image is outlined in black. **D:** Log-log plot of average final ripple amplitude $\langle a_i \rangle$ *vs.* average final wavelength $\langle w_i \rangle$ for each generation $i$. Fig. 2 labels all of the ripples analyzed in panel D. Error bars are standard deviations, and numbers of measurements are $N_0 = 1$, $N_1 = 5$, $N_2 = 6$. Lily sizes limit observable length scales to one order of magnitude. To see this figure in color, go online.

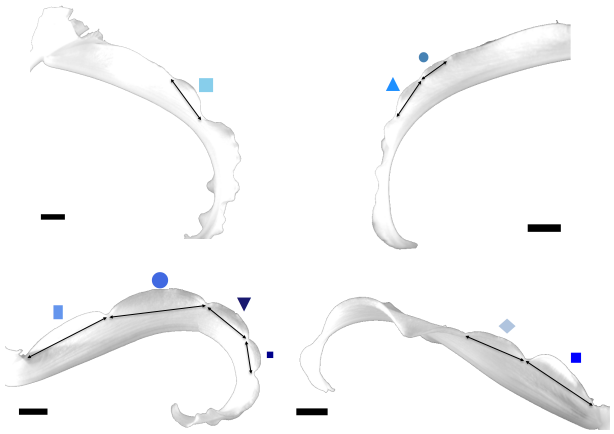

Figure 2: **Photograph with symbols marking all simple, first-generation lily tepal ripples that were evaluated.** Ripples were evaluated if they were smooth (*i.e.* without smaller, second-generation ripples) and if their white edges were imaged against a dark background rather than against another part of the white tepal, which made them straightforward to track automatically. Symbols for each ripple correspond to multiple data points through time in Fig. 3-4 and Figs. S3-S4. In all cases, tepal stems are toward the figure edges. Scale bars are 1 cm. To see this figure in color, go online.

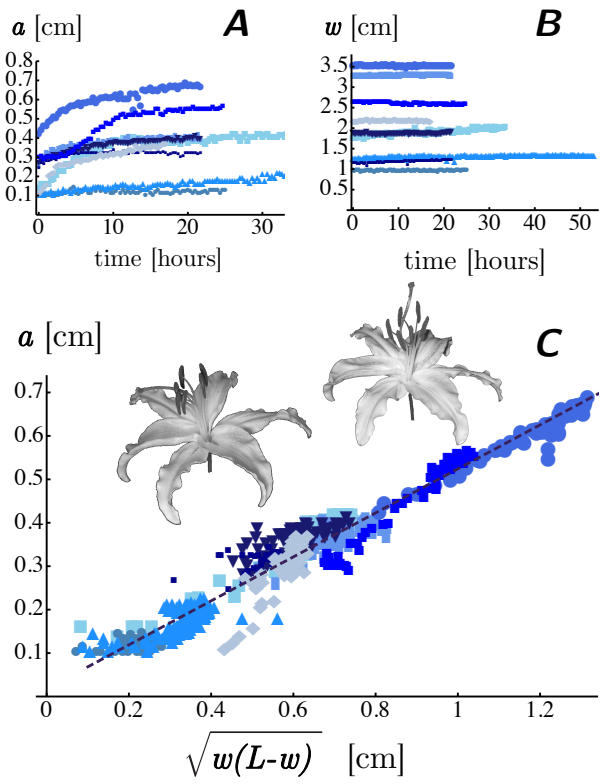


Figure 3: **Relationships between amplitude $a$, wavelength $w$, and arc length $L$ for nine first-generation ripples in lily tepals.** Fig. 2 contains images of all ripples analyzed for this figure. Each ripple is identified by a different symbol and generates many data points as the ripple changes shape over time. **A:** Amplitude increases with time (as does arc length, see large-format graphs in Fig. S4). **B:** In contrast, wavelength $w$ remains approximately constant over time. **C:** Within uncertainty, all data collapse onto a straight line when plotted as $a \propto \sqrt{w(L-w)}$. For clarity, this figure displays data for only single ripples with no superimposed higher generation ripples, excludes ripples with amplitudes $\leq 0.1$ cm, and does not show experimental uncertainties. Full data sets with experimental uncertainties appear in Fig. S3. To see this figure in color, go online.

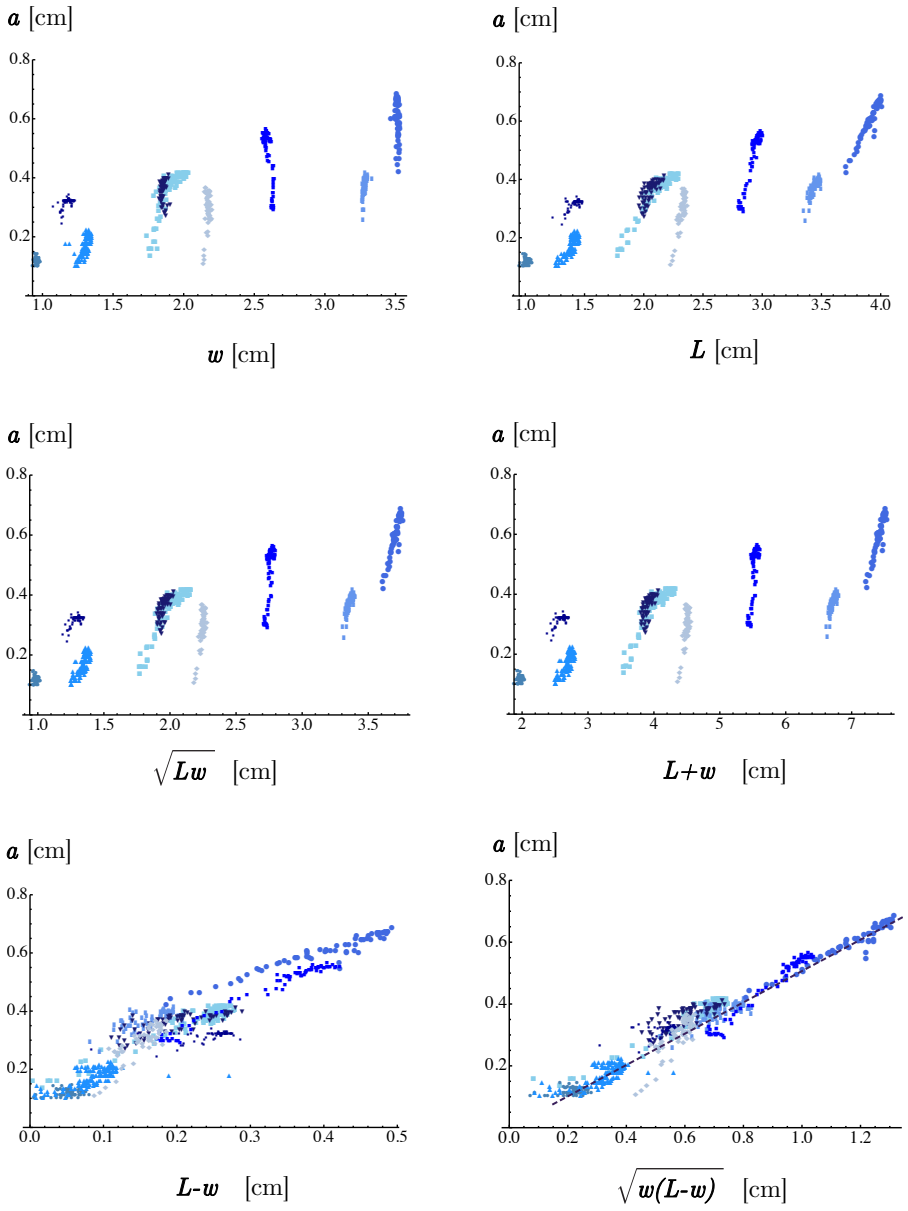


Figure 4: **Examples of scaling relationships.** Data from time-lapse movies of the tepals in Fig. 2 are plotted in six simple relationships between $a$ and $d$, where $d$ is a distance constructed from various manipulations of $w$ and $L$. For example, the top left panel shows $a$ vs. $w$, the same relationship in Eq. 1. The next three plots yield similarly poor correlation between $a$ and $d$, where $d = L$ (top right), $d = \sqrt{Lw}$ (middle left), and $d = L + w$ (middle right). A better collapse of the data onto a line is found for $a$ vs. $L - w$ (bottom left). The best collapse is found for $a$ *vs.* $\sqrt{w(L-w)}$, the equation for buckling in Eq. 2 (bottom right). To see this figure in color, go online.

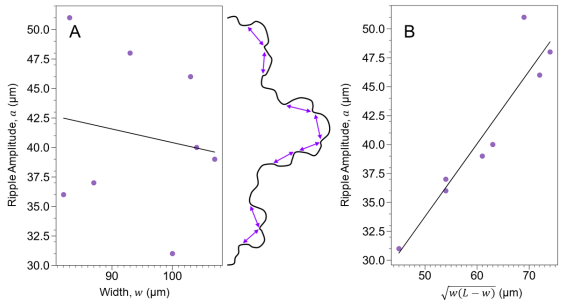


Figure 5: **Tests of relationships between amplitude $a$, wavelength $w$, and arc length $L$ for single ripples in plastic sheets.** The sketch at the center represents single, 5th-generation ripples ($N = 8$) in a plastic sheet viewed from the edge (adapted from (*9*) as in Fig. S5-S6). **A:** The shapes of these ripples are fit poorly by a line of $a \propto w$ (slope = -0.12, confidence interval = $\pm$0.27). **B:** The same ripple shapes are fit well by $a \propto \sqrt{w(L-w)}$, (slope = 0.63, confidence interval = $\pm$0.095. To see this figure in color, go online.

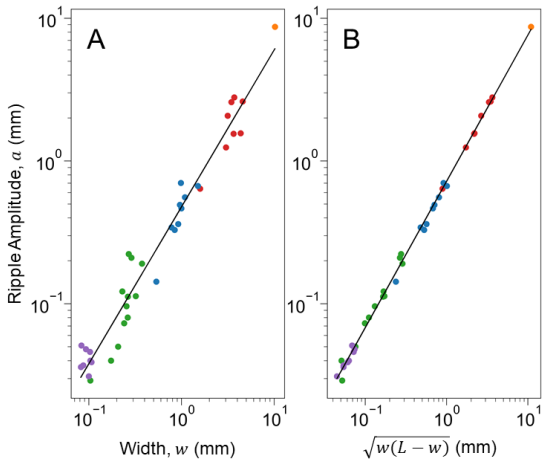


Figure 6: **Tests of relationships between amplitude $a$, wavelength $w$, and arc length $L$ for five generations of ripples in torn plastic sheets from original data in (*9*).** Each point represents an individual ripple (rather than an average), and colors correspond to successive generations of ripples in Fig. S6. **A:** The data fall roughly along a line when plotted as $a \propto w$ (on a log-log plot), with a slope of 1.1 and a confidence interval of $\pm 0.037$. **B:** The same data collapse more fully onto a line when plotted as $a \propto \sqrt{w(L-w)}$ (on a log-log plot) with a slope of 1.0 and a confidence interval of $\pm 0.0083$. To see this figure in color, go online.

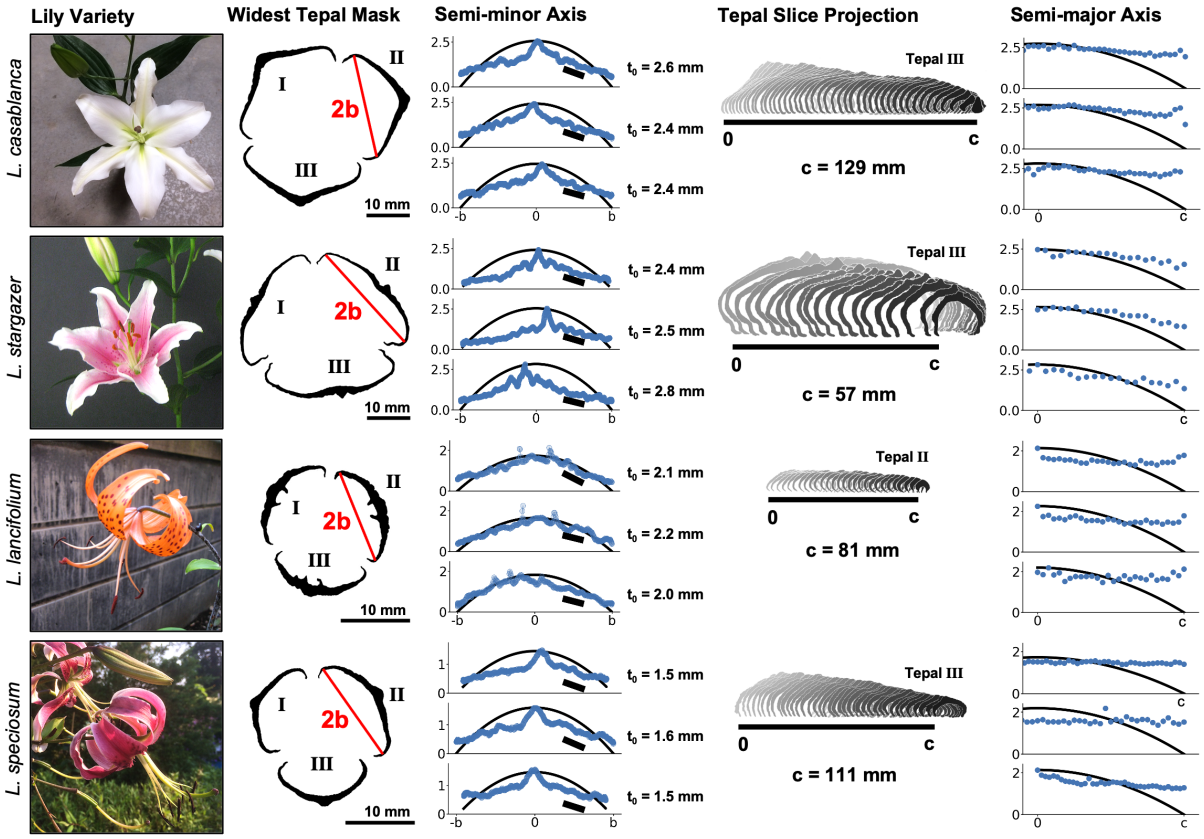


Figure 7: **Shapes of lily buds.** Column 1: Photos of blooms of four lily varieties. Column 2: Binarized masks of slices through the three outer tepals at $x = 0$ for each variety. The red line shows the semi-minor axis (from $y = -b$ to $+b$) of tepal II. A set of 24 slices for *L. Lancifolium* is shown in Fig. S7. Column 3: Tepal thicknesses in millimeters ($y$-axis) are plotted against their corresponding location on the semi-minor axis ($x$-axis). The profiles show a central peak with thickness $t_0$ due to the woody spine. Thicknesses typically decrease at least as fast as $t = t_0(1 - y^2/b^2)$ (thin black curve). Short black lines show the slope away from the woody spine. Column 4: Projection of slice masks for one of the three outer tepals of each variety. The mask at $x = 0$ is at the left, and the mask at $x = c$ is at the right. Column 5: Tepal thicknesses at $y = 0$ are roughly constant or decrease slowly along the semi-major axis (from $x = 0$ to $+c$). The y-axis is in millimeters. To see this figure in color, go online.

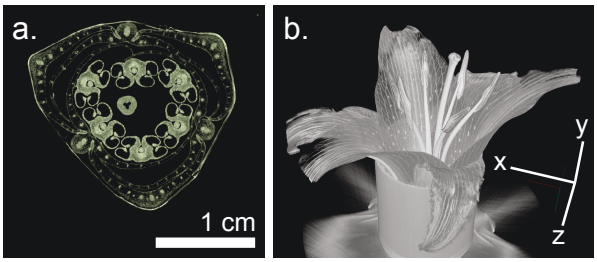


Figure 8: **X-ray tomogram and reconstruction.** (a) Slice from an X-ray tomogram of a lily (oriental hybrid). Visible structural elements include, from the outside to the center: the three outer tepals, the three inner tepals, six anthers, and the style. (b) 3-dimensional reconstruction of a lily bloom of the same variety. The tilt of the reconstruction is shown by the axes. To see this figure in color, go online.